Hindawi
Advances in Materials Science and Engineering
Volume 2018, Article ID 3929682, 13 pages
https://doi.org/10.1155/2018/3929682

Research Article

Investigation of Cement-Emulsified Asphalt in Plastic Concrete

Xiaohu Yan,[1,2] Zaiqin Wang,[1,2] Meijuan Rao,[3] and Mingxia Li[2]

[1]*College of Water Conservancy and Hydropower Engineering, Hohai University, Nanjing 210098, China*
[2]*Yangtze River Scientific Research Institute, Wuhan 430010, China*
[3]*State Key Laboratory of Silicate Materials for Architecture, Wuhan University of Technology, Wuhan 430070, China*

Correspondence should be addressed to Meijuan Rao; raomeijuanding@163.com

Received 22 December 2017; Accepted 8 March 2018; Published 3 April 2018

Academic Editor: Lijing Wang

The mechanical, mesodamage, and the microproperties of cement-emulsified asphalt concrete have been investigated by computed tomography (CT), scanning electron microscopy (SEM), X-ray diffraction (XRD), and thermogravimetric analysis (TG) in this work. Emulsified asphalt delayed the hydration of cement, making the early compressive strength of concrete develop slowly. However, the concrete compressive strength increased rapidly with the demulsification of emulsified asphalt. The damage stages of condense, expansion of volume, rapid crack propagation, and damage by real-time scanning have been observed. The CT mean value of the place near the lower end face suffered a larger decline but a smaller decline to the upper part of the sample. The evolution of concrete suffering damage to failure is a gradual development process, and no sharp expansion of brittle failure. The unhydrated cement, incorporation asphalt, fibrous C–S–H gel, CH, needle-shaped ettringite, and other hydration products were interwoven to constitute emulsified asphalt-cement paste, forming a spatial structure.

1. Introduction

With the development of social productive forces, there is a gradual improvement in the quality of material used for constructing buildings. However, there are still some limitations in the building materials, leading to hindrances in the development of strong structural forms. Superior construction methods cannot be implemented completely due to these limitations of the building material. Many technical problems of construction engineering are currently being solved, thanks to the breakthrough achieved in the synthesis of building materials [1]. According to statistics, seepage plays an important role in the destruction of earth-rock dams, indicating that it is very important for improving the quality of earth-rock dams and preventing leakage. At present, there are two problems that should be solved urgently. These problems are caused by the impervious wall in dyke projects; therefore, the traditional building materials must be updated with sophisticated technology. First problem is to develop antiseepage measures to avoid the reinforcement of dangerous reservoirs. Second problem is to effectively suppress the high pressure of earth-rockfill dam, which is caused by the deep foundation of the covering layer. To solve all these issues, we should judiciously select the impervious materials.

The plastic concrete is a kind of flexible material with moderate properties, so it can be considered as a building material whose quality is somewhere between the soil and the ordinary concrete. This novel material is used to solve the problems faced while using the common concrete cutoff wall [2]. Presently, most of the impervious core wall materials are made of plastic concrete or asphalt concrete in order to improve the impermeability of the impervious wall and to reduce the elastic modulus of the concrete. In general, plastic concrete always contains certain characteristic toughening components, such as bentonite or clay composite bentonite. By incorporating these toughening components, we substantially improve the crack resistance and impermeability of concrete. With this strategy, we also ameliorate the workability and fluidity of concrete. Thus, we make concerted efforts to reduce the cement consumption and concrete cost [3–6]. The characteristics of plastic concrete are as follows: its elastic modulus is relatively low, and the value of this parameter is very close to the elastic modulus of dam

Table 1: Properties of emulsified asphalt.

Items	Results	Technical requirements of hydraulic asphalt SG90 by GB 50092-1996	Performance standards
Needle penetration (25°C, 100 g, 5 s) (0.1 mm)	95.5	80~100	DL/T 5362-2006
Softening point (ring and ball method) (°C)	43.2	42~52	
Ductility (15°C, 5 cm/min) (cm)	160	≥100	
Density (25°C) (g/cm^3)	1.01	Measured data	
Solubility (%)	99.6	≥99.5	
Flash point (°C)	290	≥230	

Table 2: Chemical composition of cement, fly ash, and clay (%).

Items	SiO_2	Fe_2O_3	Al_2O_3	CaO	MgO	f-CaO	K_2O	Na_2O	R_2O	SO_3	Loss
Cement	21.7	5.0	4.1	62.1	4.8	0.1	—	—	—	0.7	0.2
Fly ash	59.0	8.8	21.6	5.1	1.5	—	0.8	0.2	0.7	0.6	1.4
Clay	55.6	5.9	15.0	5.6	4.6	—	—	—	—	—	—

body and foundation. Furthermore, the ratio of elastic modulus to strength is generally lower than 500; however, the permeability and durability are limited. The permeability coefficient is generally in the range of 10^{-7} cm/s, and the compression strength generally ranges between 2 MPa and 5 MPa in the ageing period of 28 days. In the traditional impervious wall made from plastic concrete, the compressive strength is not that high. To tackle this issue, we conducted sufficient research on how to improve durability of the material. The traditional material is mostly used for constructing impervious cofferdams that sustain for a temporary period. The traditional material is also used for constructing permanent structures having the foundation of low dam and thin overburden. In this paper, we address the deficiency of traditional plastic concrete in order to synthesize a better material that is a good match of different strength grades of concrete. Our aim is to improve the plasticity of the concrete structure; therefore, the new toughening components of emulsified asphalt have been added to plastic concrete [7]. Based on the results of experimental analysis, we propose that plastic concrete should be used for constructing the permanent impervious wall under deep overburden foundation; the same wall may also be built with plastic concrete of high anticracking site, and so on. Thus, we can effectively solve the major technical problems of hydraulic concrete, such as cracking resistance. Our main purpose is to prevent permeability in order to improve the service life of hydraulic structures.

2. Experimental

2.1. Raw Materials. Cationic emulsified asphalt, Huaxin 42.5 moderate heat Portland cement, clay of a project, Xuanwei grade I fly ash, Jiangsu Bote JM PCA high-efficiency water-reducing agent and GYQ air entraining agent, artificial marble sand, and artificial sandstone rubble were used in this study. The testing result showed that the raw materials meet the relevant technical requirements. Properties of emulsified asphalt and chemical composition of raw materials are shown in Tables 1 and 2.

2.2. Experimental Methods. Experimental methods and data analysis methods in this study were according to SL 237-99 specification of soil test, and SL 352-2006 test code for hydraulic concrete, DL/T5150-2001 specification of concrete cutoff wall used for hydropower and water conservancy project, and DL/T 5330-2015 code for mix design of hydraulic concrete. Different water-binder ratios (0.3, 0.45, and 0.6), asphalt-cement ratios (0, 0.4, and 0.6), and the clay contents (0%, 20%, and 40%) were considered in the test. The content of fly ash was 15%. For explaining its effects on macroscopic mechanical properties, combined with microtesting methods such as CT, XRD, SEM, TG-DSC, and so on [8], microtopography and chemical composition of hydration products of cement-emulsified asphalt slurry were investigated.

CT scanning technology relies on the principle that the degree of attenuation of radiation passing through the medium is proportional to its density. It combined with computer technology and image processing technology; the physical internal density information will be obtained by digital image reflecting. Shape, internal structure, and composition of the material can be recognized based on the density-related image information. Density information of the CT images shows the gray area of information packets.

CT essentially involves a two-dimensional distribution of a physical quantity in the fault area. The physics is that the linear attenuation coefficients $\mu(x, y)$ and $\mu(x, y)$ are directly related to the density of the object. In the early times, CT technology workers were defined as the standard CT number Hp by the attenuation coefficient of water, which was expressed as

$$\mathrm{Hp} = \frac{\mu_m - \mu_w}{\mu_w} \times 10^3, \quad (1)$$

where μ_w and μ_m are the attenuation coefficients of water and the medium, respectively.

The CT number of each pixel can be obtained through (1). Each CT number corresponds to a gray value; thus, a tomographic gray scale digital matrix is formed. The CT testing machine will get a set of CT gray scales by continuously scanning objects in the vertical cross-sectional direction.

Table 3: Mix proportion parameters of cement-emulsified asphalt concrete.

Samples	Water-binder ratio	Emulsified asphalt-binder ratio	Clay (%)	Fly ash (%)
Xq1	0.30	0.4	20	15
Xq2	0.30	0.6	20	15
Xq3	0.45	0	0	15
Xq4	0.45	0	20	15
Xq5	0.45	0.4	0	15
Xq6	0.45	0.4	20	15
Xq7	0.45	0.4	40	15
Xq10	0.45	0.6	20	15
Xq12	0.60	0.4	20	15
Xq15	0.60	0.6	20	15

Table 4: Mix proportion parameters of cement-emulsified asphalt concrete for the microtest.

Samples	Water-binder ratio	Fly ash (%)	Clay (%)	Emulsified asphalt-binder ratio
X0	0.45	15	0	0
X1	0.45	15	0	0.4
X2	0.45	15	20	0
X3	0.45	15	20	0.4

These gray scales will get the whole composition of the interior of the space in the object through three-dimensional reconstruction. Threshold values for each phase medium and CT number of concrete specimens are hardened cement mortar (2000~2200), aggregate (2200~3071), and interfacial transition zone (1000~1600). Mix proportion parameters of cement-emulsified asphalt concrete and mix proportion parameters of cement-emulsified asphalt concrete for the microtest are shown in Tables 3 and 4.

3. Results and Discussion

3.1. The Influence of Water-Binder Ratio on Properties of Cement-Emulsified Asphalt Concrete. Properties of the cement-emulsified asphalt concrete with the water-cement ratios of 0.3, 0.45, and 0.6, respectively, are shown in Table 5.

The results indicate the following effects:

(1) The compressive strength of cement-emulsified asphalt concrete decreased gradually with the steadily increasing water-cement ratio. Compared to the initial phase, the water-binder ratio exerted a slightly greater impact on the compressive strength of concrete at the later stage. This was the result of incorporating emulsified asphalt and clay in order to reduce the dosage of cement in concrete. As a result, there was considerable reduction in the posthydration products. With a large amount of emulsified asphalt, we could significantly alter the strength of concrete. The larger the amount of emulsified asphalt, the lower the compressive strength of concrete would be. The composition and performance of emulsified asphalt was commendable in changing the compressive strength of concrete.

(2) The splitting tensile strength and the tensile strength of emulsified asphalt concrete were reduced by steadily increasing the water-cement ratio. For the concrete, the ratio of compressive strength to the splitting tensile strength was in the range 9.6–11.3. The higher the concrete strength, the greater the ratio would be. In cement-emulsified asphalt concrete, the ratio of compression to tension was slightly lower than the value of ordinary concrete. This indicates that cement-emulsified asphalt concrete had some level of plasticity. The splitting tensile strength was higher than the axial tensile strength. In concrete material, the ratio of splitting tensile strength and axial tensile strength was in the range 1–1.11 on the 28th day; the same ration was in the range 1.08–1.32 on the 90th day. This ratio increased gradually with the increasing age of concrete.

(3) The water-binder ratio had some significant influence on the compressive elastic modulus of cement-emulsified asphalt concrete; the compressive elastic modulus increased when the water-cement ratio decreased steadily; the decline in the water-cement ratio was achieved by increasing the compressive strength of cement-emulsified asphalt concrete.

3.2. Influence of Different Dosages of Emulsified Asphalt on Concrete Properties. The ratio of modulus to strength indicates the internal relationship between the characteristics of tensile strength and elastic modulus of concrete; the modulus is an important index to assess the plasticity of emulsified asphalt concrete [9]. The test results indicate that except for the Xq1 specimen, the elastic moduli of cement-emulsified asphalt concrete specimens were all below 5.2 GPa on the 90th day. The ratio of modulus to strength of concrete was relatively low. In general, this ratio was less than 500. Under some circumstances, it was even below 200. The results indicate that the deformation capacity of emulsified asphalt concrete is greater than the ordinary hydraulic concrete. Therefore, cement-emulsified asphalt concrete has excellent toughness when it is treated with moderate compressive concrete.

Table 6 indicates that the compressive strength, splitting tensile strength, and the tensile strength of cement-emulsified asphalt concrete decreased gradually when we steadily increased the content of emulsified asphalt. In this case, there was sharpest reduction in the compressive strength of concrete; however, the growth rate of long-term strength was higher than that of undoped emulsified asphalt concrete. For emulsified asphalt concrete, the ratio of modulus to strength was significantly lower than the concrete devoid of emulsifying asphalt.

The hydration of cement was delayed by incorporating emulsified asphalt, making concrete own retarding property. This phenomenon can be explained as follows: the emulsified asphalt contained a high amount of water; the water was released after demulsifying the previously emulsified asphalt. The resultant asphalt subsequently participated in the hydration of cement. On the other hand, some bitumen-coated

Table 5: Properties of cement-emulsified asphalt concrete under different water-binder ratios.

Samples	Compressive strength (MPa)			Splitting tensile strength (MPa)			Elastic modulus (GPa)			Tensile strength (MPa)	
	14 d	28 d	90 d	14 d	28 d	90 d	14 d	28 d	90 d	28 d	90 d
Xq1	6.7	9.5	15.1	0.64	0.93	1.33	2.96	4.81	10.53	0.88	1.04
Xq6	5.6	8.2	13.3	0.55	0.80	1.19	2.48	3.53	5.14	0.73	0.90
Xq12	4.8	7.2	10.5	0.50	0.70	1.00	1.16	3.04	4.53	0.65	0.85
Xq2	4.1	5.4	7.7	0.38	0.53	0.70	1.98	2.48	3.07	0.50	0.65
Xq10	3.6	5.0	6.9	0.34	0.50	0.68	1.15	2.18	3.16	0.45	0.57
Xq15	3.2	4.0	5.9	0.30	0.38	0.60	0.62	1.01	1.68	0.38	0.50

Table 6: Concrete properties under varying dosages of emulsified asphalt (water-cement ratio 0.45).

Samples	Compressive strength (MPa)			Splitting tensile strength (MPa)			Elastic modulus (GPa)			Elastic modulus and compressive strength ratio			Tensile strength (MPa)	
	14 d	28 d	90 d	14 d	28 d	90 d	14 d	28 d	90 d	14 d	28 d	90 d	28 d	90 d
Xq4	13.5	20.8	24.4	0.90	1.60	2.00	12.15	17.79	19.87	900	855	814	1.10	1.78
Xq6	5.6	8.2	13.3	0.55	0.80	1.19	2.48	3.45	5.14	442	430	387	0.75	1.10
Xq10	3.6	5.0	6.9	0.34	0.50	0.68	1.15	2.18	3.16	319	436	485	0.56	0.65

cement particles and hydration products significantly alter the concrete structure, eventually reducing the interfacial bonding strength of the concrete, leading to a decrease in the early strength of the concrete.

3.3. Influence of Varying Dosages of Clay on Concrete Properties. In plastic concrete, the toughening component is clay as it is able to improve the deformation property of plastic concrete. After mixing emulsified asphalt concrete with clay, we investigated the properties of the mixed material. Thus, we analyzed the influence of varying the dosages of clay on the properties of cement-emulsified asphalt concrete. To obtain the correct mix proportion of emulsified asphalt concrete, we strictly maintained the following parameters: the water-binder ratio of 0.45, the asphalt-cement ratio of 0.4, and the clay content of 0%, 20%, and 40%, respectively. Table 7 presents the test results of this analysis.

The results indicate that clay reduces the elastic modulus of cement-emulsified asphalt concrete. Except for the Xq7 specimen, the ratios of modulus to strength were below 500 for all the specimens. The compressive strength of the Xq6 specimen reached 8.0 MPa, and the ratio of modulus to strength was 430 on the 28th day. When clay is incorporated into plastic concrete, its strength is significantly increased compared to clay-free samples. In both cases, we maintain the same modulus ratio [10].

By increasing the content of clay in cement-emulsified asphalt concrete, it a gradual decrease in the following parameters is observed: the compressive strength, the splitting tensile strength, and the tensile strength. The effect of clay was quite significant on the late compressive strength of concrete. The late growth of splitting tensile strength was faster in cement-emulsified asphalt concrete. In contrast, the late growth of axial tensile strength was slower in cement-emulsified asphalt concrete. Strength was low when cement emulsion asphalt mixed with clay. This is caused by the inert nature of the clay and the retardation of the emulsified asphalt. By adding clay to the concrete, we have significantly reduced the amount of equivalent cement. As a result, the amount of cement hydration produced is also small. These changes weaken the cementing capacity of gravel aggregates and result in a thinner network structure than normal concrete. All these undesirable reactions led to a significant reduction in the strength of concrete.

3.4. Computed Tomography (CT). The concrete specimen Xq6 was selected to calculate the CT mean value of each section subjected to continuous loading [11–13]. We successfully obtained the CT mean value of each section. Figure 1 illustrates the following developments in the CT scan of the specimen: seven sections were selected along the concrete column; the cross-sectional area was 66.50 cm^2, and the spacing for each section was 25 mm. Figure 2 illustrates the gray scale CT scan of each concrete section under different stress. Figures 3(a) and 3(b) illustrate the CT mean values curve of each section subjected to continuous load.

As can be seen in Figures 3(a) and 3(b), the three sections of cement-emulsified asphalt concrete were not damaged, but the other four sections were destroyed seriously. This occurred due to the low strength and plasticity of cement-emulsified asphalt concrete. There was relatively small variation in the CT mean values of the first three sections when they were subjected to different loads. This indicates that the state of concrete altered due to compaction and microdilatancy. In the other four sections of the sample, we observed four different concrete damage evolutions: the compaction of each section increased dramatically as we steadily increased the load. This leads to an increase in the density and CT average of cement-emulsified asphalt concrete. When the load was increased to 5.15 MPa, we observed that the CT value of each section started declining slightly. This indicated the initial stage of concrete damage. When we

Table 7: Concrete properties under varying dosages of clay.

Samples	Clay (%)	Compressive strength (MPa)			Splitting tensile strength (MPa)			Elastic modulus (GPa)			Elastic modulus and compressive strength ratio			Tensile strength (MPa)	
		14 d	28 d	90 d	14 d	28 d	90 d	14 d	28 d	90 d	14 d	28 d	90 d	28 d	90 d
Xq5	0	9.2	11.1	16.7	1.00	1.10	1.40	1.97	4.02	7.32	213	362	438	0.95	1.28
Xq6	20	5.6	8.2	13.3	0.55	0.80	1.19	2.48	3.53	5.14	442	430	387	0.75	1.10
Xq7	40	3.1	4.2	6.3	0.20	0.40	0.60	0.83	1.57	3.58	268	374	568	0.40	0.55

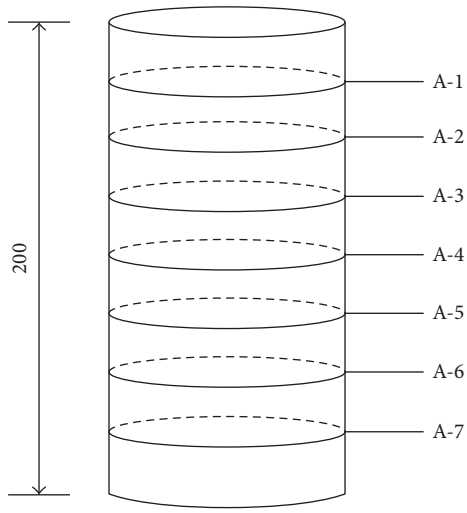

Figure 1: Cross sections of cement-emulsified asphalt concrete (size: mm).

increased the limit load to 5.44 MPa, we observed the development of microcrack for the first time. Subsequently, the expansion was substantially enough to accelerate the damage. Then, we observed too many cracks developing in the specimen within a very short period of time. However, there was significant reduction in the volume of specimen expansion, the rapid diminution of the density, and the CT mean value. Finally, we destroyed the lower section of the specimen by increasing the load to 5.30 MPa.

3.5. Analysis of Binary Image. In the mathematical morphology method, we used integral geometry to define geometrical parameters, which were then used to indirectly measure and characterize irregular geometric shapes. Moreover, the random nature of the image was comprehended by random set theory of the method [14–17]. Therefore, it can be used to quantitatively describe CT images of concrete structure. To determine the variation in each pixel gray value and to estimate the crack criterion for each pixel gray value, we used the following equation:

$$H_{i,j} = \max\left(H_{i,j}, H_{i+1,j}, H_{i,j+1}, H_{i+1,j+1}\right), \quad (2)$$

where $H_{i,j}$ is the CT gray value of the i line and j column pixel, $i, j = 1, 2, 3, \ldots, 1024$. All the image data are represented by 0 and 1; therefore, you can extract the crack by setting a gray threshold as follows: when the intensity is greater than the threshold indicated by 1 or is less than the threshold indicated by 0. The data matrix of a gray scale image representing 1-pixel size was considered as a unit for statistics; it was substituted into the equation to extract threshold ξ at a certain crack, so it can be realized through binarization of the cracked image, namely, crack extraction. When $H_{i,j} < \xi$, the points are included in the crack area; when $H_{i,j} < \xi$, the points are included in the noncracked area. Figure 4 and Table 8 present the test results of this analysis.

Figure 5 illustrates that there are many cavities in the cement-emulsified asphalt concrete specimens; these cavities have an uneven size in the specimens. In the cement-emulsified asphalt concrete specimens, stress concentration occurs easily and a crack initiation point develops. These undesirable events ultimately lead to widespread cracks that damage the specimen completely.

By examining the CT scan binary image, we can summarize the development trend of the crack in each section of the specimen. In the concrete section A-7, we observed continuous cracks at the microscopic level. However, other sections did not form continuous crack until the loading was increased to 4.9 MPa. In this period, the concrete exhibited alternating stages of compaction and microdilatancy. These observations complied with the results of CT number analysis. When the load was increased continuously, we observed the gradual development of crack in section A-7. First, only two continuity cracks were observed at the edge of the section. The crack width subsequently increased. At the same time, scattered fine cracks were observed in the middle of the cross section, which correlates with the formation at the crack edge. All these cracks substantially destroyed the section of concrete. Based on these observations, we infer that the concrete crack was caused by the hole present in sections A-4 and A-6. When the load was increased to 5.44 MPa in section A-4, we observed intermittent microcracks. Furthermore, we observed continuous cracks when the load was increased to 5.30 MPa. Near the hole, stress concentration appeared when the section A-6 was subjected to stress. Thus, the development of cracks was rapid, extending into the weak zone of the concrete structure. All these developments resulted in the separation of cementitious materials and aggregates at the interface. Such closely connected, adjacent cracks were observed in an interlaced and interconnected fashion, leading to the development of crack propagation. Crack stress unleashed rapidly with the propagation of cracks. When the load was increased in definite increments, we could not observe continuous cracks in the section A-2; the section was minutely examined by the CT image intuitive method.

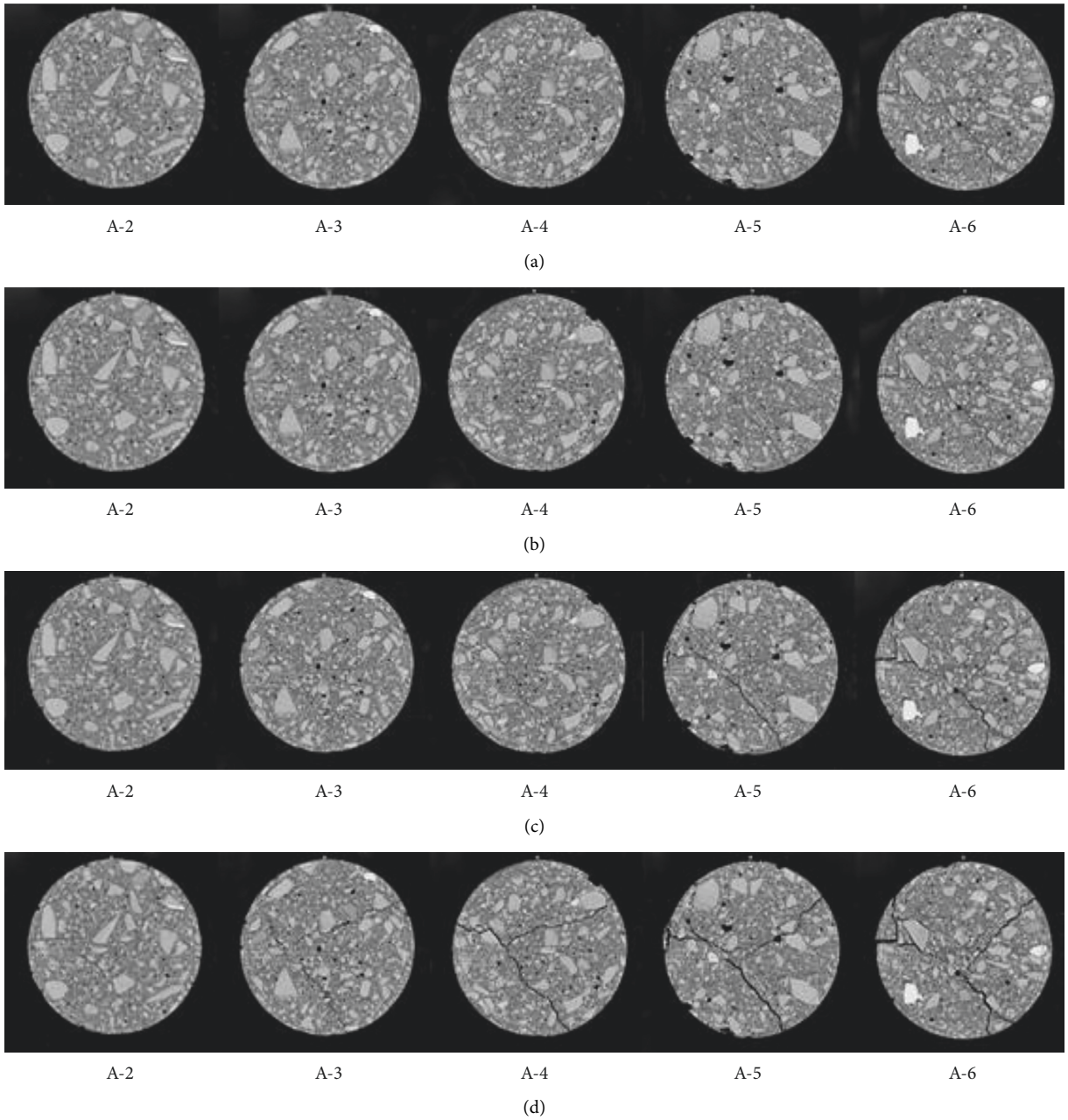

Figure 2: Gray CT picture of concrete cross section under various stresses (28d). (a) $\sigma = 3.18$ MPa, (b) $\sigma = 5.15$ MPa, (c) $\sigma = 5.44$ MPa, and (d) $\sigma = 5.30$ MPa.

However, a small piece of continuous crack was detected when we implemented the binary image analysis method on the section exposed to the ultimate load, and the continuous crack developed due to low compressive strength and a certain amount of toughness in cement-emulsified asphalt concrete.

When the cement-emulsified asphalt concrete was subjected to the ultimate load, we observed fine cracks in the upper section; however, these cracks were observed because the upper part was experiencing alternating states of compaction and expansion. Based on these observations, we conclude that a lot of voids had developed in the cement-emulsified asphalt concrete. These cracks were immensely useful in dissipating the external pressure. Furthermore, the toughness of the material increased tremendously when the concrete was mixed with the emulsified asphalt and the clay-toughening component; therefore, the novel hybrid material was experiencing alternating states of compaction, expansion, reconsolidation, and reexpansion when subjected to increasing amounts of load. In the specimen, we mainly observed small cracks and discontinuous cracks. In other words, the specimen does not crack even when subjected to an increased load. In the middle and lower parts, we observed a large connectivity crack under the action of failure load; however, penetrating crack was not observed in the upper and lower layers.

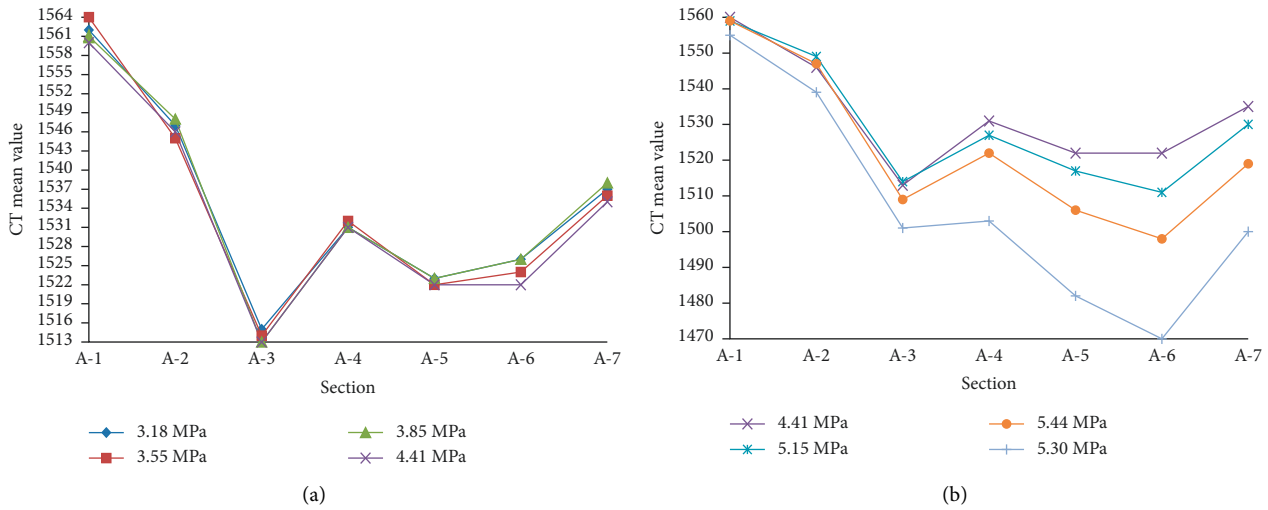

Figure 3: (a) CT mean value comparison of each cross section under continuous loading (3.18 MPa, 3.55 MPa, 3.85 MPa, and 4.41 MPa). (b) CT mean value comparison of each cross section under continuous loading (4.41 MPa, 5.15 MPa, 5.44 MPa, and 5.30 MPa).

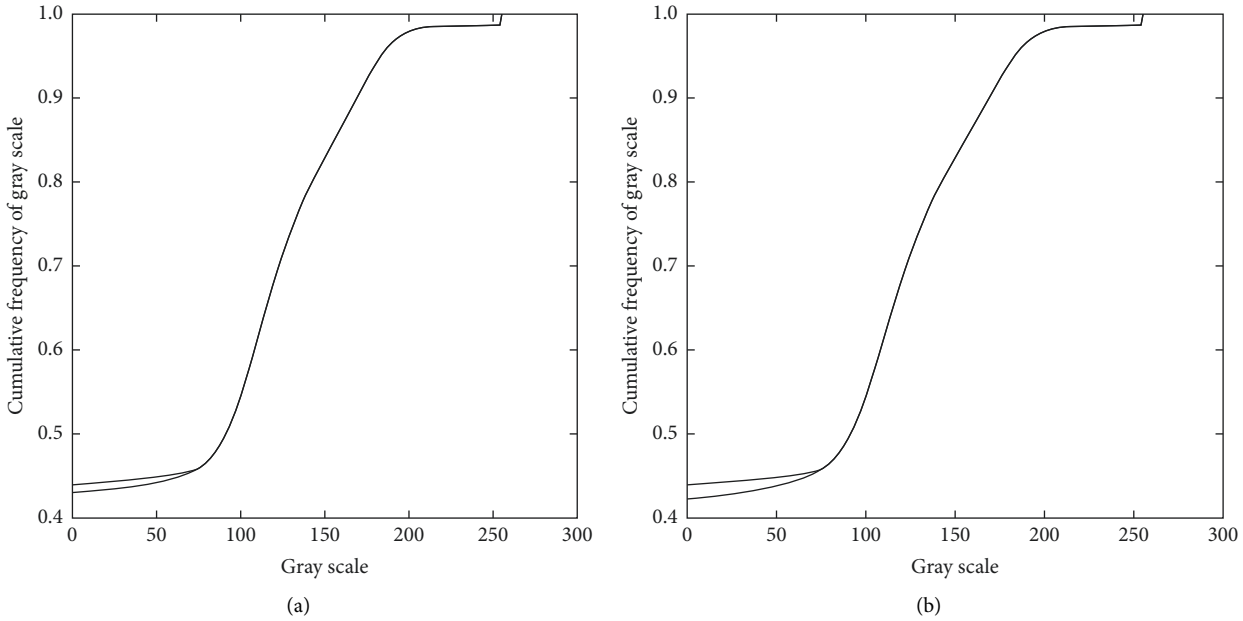

Figure 4: (a) Cumulative frequency of gray scale with the load of 5.44 MPa and 3.18 MPa under section A-7 of Xq6. (b) Cumulative frequency of gray scale with the load of 5.30 MPa and 3.18 MPa under section A-7 of Xq6.

Table 8: Binary analysis threshold of each section of Xq6.

Sections	5.15 MPa to 3.18 MPa	5.44 MPa to 3.18 MPa	5.30 MPa to 3.18 MPa	Mean
A-2	—	—	75	75
A-4	—	73	69	71
A-6	71	65	62	66
A-7	84	79	81	81

3.6. Scanning Electron Microscope (SEM) Analysis. The SEM images of emulsified asphalt-cement paste specimens' hydration products at 7th and 28th day of different dosage combinations as in Table 4 are shown in Figure 6.

As shown in Figure 6(a), C–S–H gel, $Ca(OH)_2$, AFt, AFm, and other hydration products were observed along with the unhydrated cement clinker particles in the undoped emulsified asphalt and clay cement at the 7th day. Moreover, the slurry was highly porous in nature. In addition, some products had not yet developed into a crystalline form completely at the 7th day: C–S–H gel was mainly type II, but it was difficult to find C–S–H gel particles of type III. There were some needle-shaped ettringite (AFt) in the holes because gypsum and lime stimulated the samples to form ettringite [18, 19] (AFt). When we increased the ageing period in definite increments, we observed that there was a decrease in unhydrated cement particles; however, the

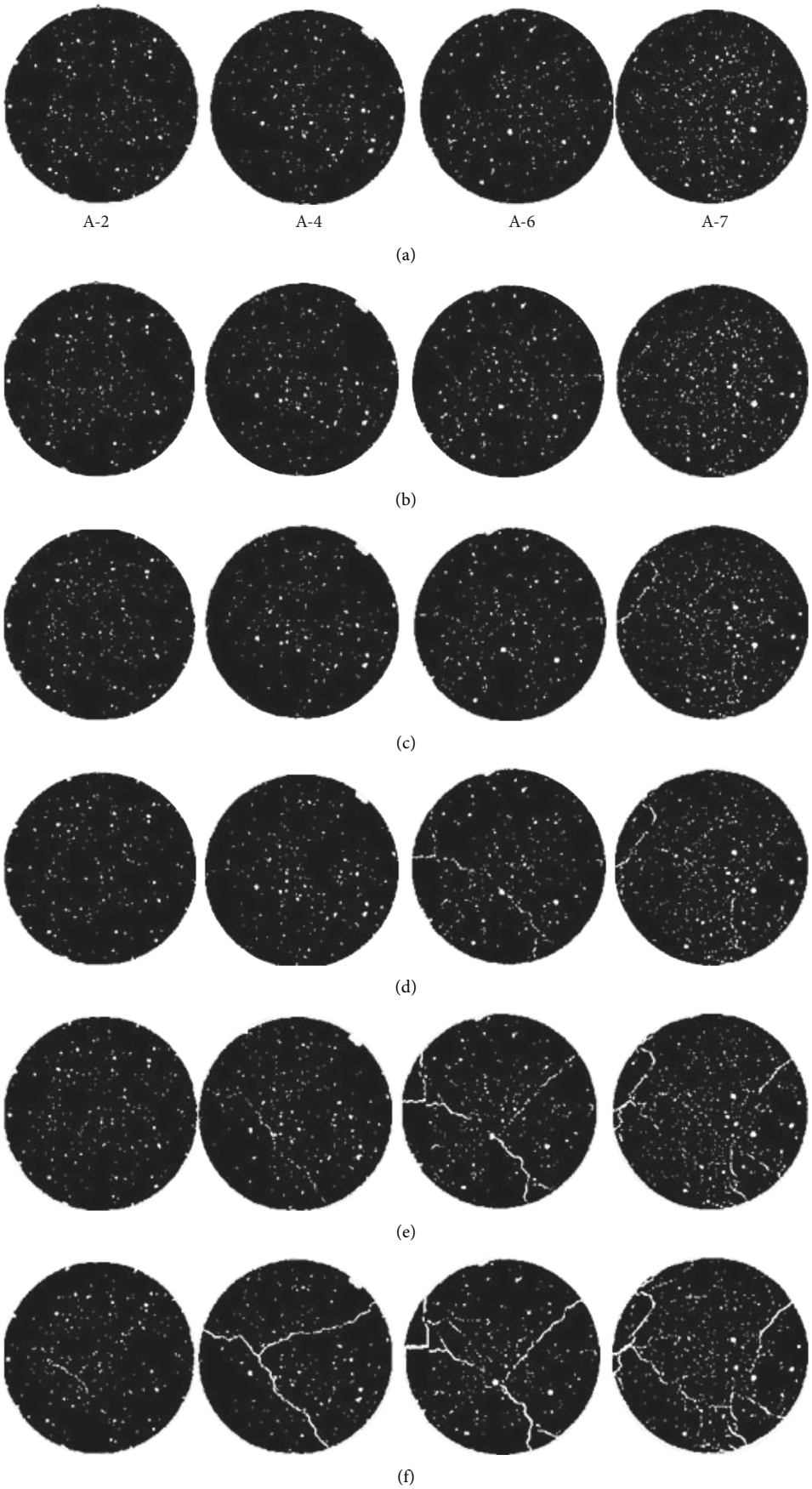

Figure 5: Binary image of the Xq6 specimen under different stress sections (28 d). (a) $\sigma = 3.18$ MPa, (b) $\sigma = 3.55$ MPa, (c) $\sigma = 4.9$ MPa, (d) $\sigma = 5.15$ MPa, (e) $\sigma = 5.44$ MPa, and (f) $\sigma = 5.30$ MPa.

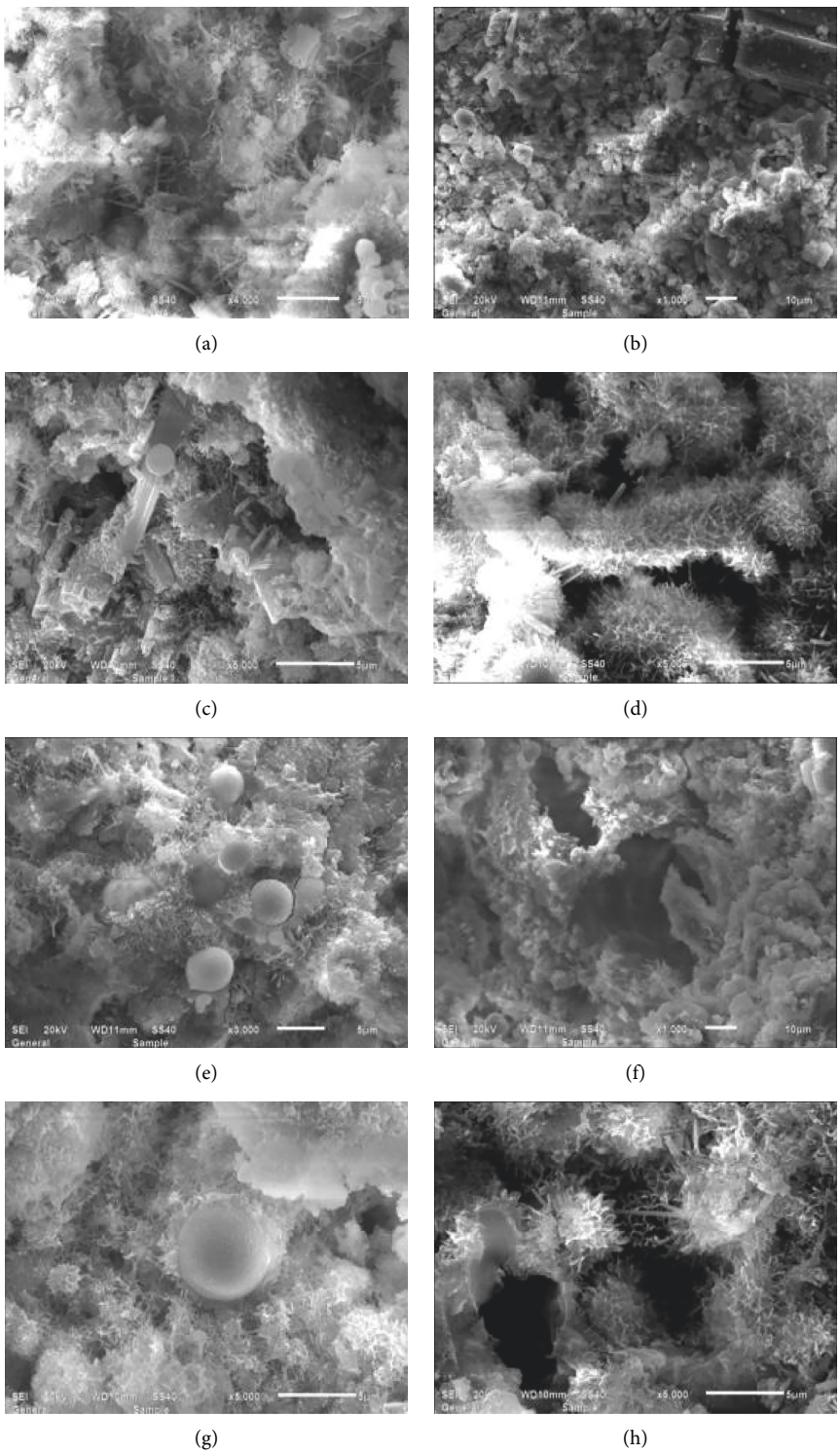

FIGURE 6: SEM images of cement-emulsified asphalt paste samples: on the 7th day, (a) without emulsified asphalt and clay, (b) with emulsified asphalt, (c) with clay, and (d) with emulsified asphalt and clay; on the 28th day, (e) without emulsified asphalt and clay, (f) with emulsified asphalt, (g) with clay, and (h) with emulsified asphalt and clay.

amount of hydration products increased simultaneously, and the structure gradually became dense. The shape of hydration products C–S–H of cement paste was approximately the same when the cement paste was mixed with single-doped emulsified asphalt [20], single-doped clay, and pure cement; the product was mainly appearing in the form of spherical C–S–H gel. Figure 6(c) illustrates the part where the clay particles fill the void, leading to the formation of a structure that is more compact than the single-doped emulsified asphalt-cement paste. Furthermore, we also

observed a small amount of needle-shaped ettringite (AFT), small pieces of plate-type $Ca(OH)_2$ crystals, and fly ash particles; the hydration products had completely wrapped these minor products. Figures 6(b) and 6(d) illustrate that the emulsified asphalt was not involved in the hydration reaction of cement; however, many pores were observed in the cement-emulsified asphalt paste. These pores were caused by the "vacancy" of bubble burst and water evaporation during the forming process. The surface of the slurry is not smooth; it is very uneven and there is a lot of bump [19, 21–23]. Asphalt particles were round in shape, with a significant portion of particles being encased with cement particles or clay particles. These factors decelerated the cement hydration rate, leading to the slow development of concrete strength.

Figure 6(e) shows the nature of products on the 28th day of ageing: hydration products were fibrous (type I), meshy (type II), and granular (type III) C–S–H gels (some type I of C–S–H gel shape were flowers). Furthermore, we also observed $Ca(OH)_2$ crystal and monosulfate calcium sulfoaluminate hydrates in the form of hexagonal flakes. Figure 6(g) shows that the clay particles were gradually surrounded by fibrous, flocculent, and layered hydration products. In addition, C–S–H gel and hydrated sulfoaluminate had intertwined with each other to form a relatively dense structure, leading to a reduction in the volume of pores. However, crystals of hydration products appeared in a haphazard arrangement. As shown in Figures 6(f) and 6(h), emulsified asphalt contains water that initiates and promotes hydration. As a result, the hydrate content gradually increases. The shape of asphalt particles had changed from a regular sphere to an irregular ball pie. These particles had got attached to the cement hydration products.

3.7. X-Ray Diffraction Analysis (XRD). The XRD patterns of emulsified asphalt-cement paste specimens' hydration products at 7th day and 28th day of different dosage combinations as in Table 4 are shown in Figures 7 and 8.

As shown in Figures 7 and 8, the hydration products of cement-emulsified asphalt paste were substantially similar even in different proportions; the main hydration products were C_2S, C_3S, $Ca(OH)_2$, and ettringite. The amount of hydration products were increasing gradually with the progress of ageing process, but a different number of hydration products were generated in different cementitious systems. The ettringite diffraction peaks of X2 and X3 specimens are higher than the peaks of X0 and X1 specimens on the 7th and 28th days of ageing.

The patterns clearly illustrate that kaolinite, quartz, and calcite were the main components of clay. By comparing the specimens X0, X2, and X3, we found that this clay was a kind of inert admixture, and it was not involved in the hydration reaction. The reaction played a significant role in generating products, which acted as fillers in the concrete. Thus, the concrete pore structure improved tremendously, and there was a sharp decline in the rate at which the load damaged the concrete. By comparing the X-ray diffraction patterns of both types (doped and undoped) of emulsified asphalt

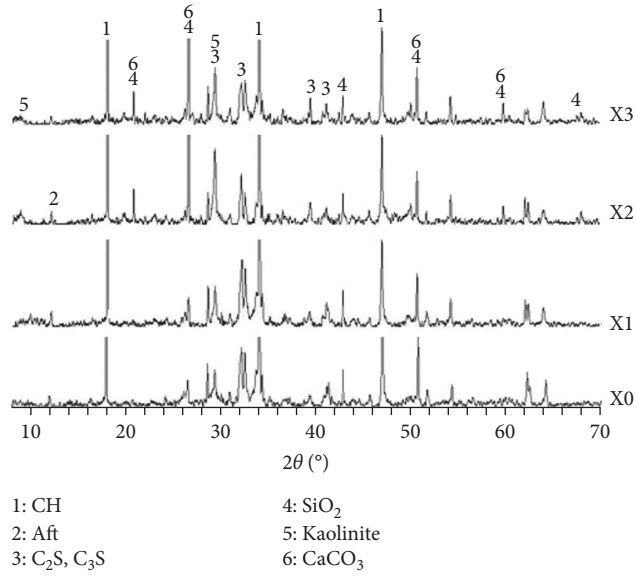

Figure 7: X-ray diffraction pattern of cement-emulsified asphalt paste under different proportions for 7 d.

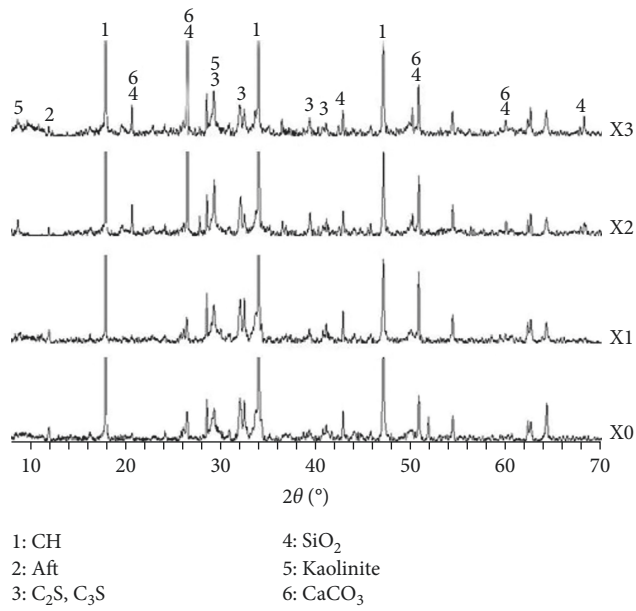

Figure 8: X-ray diffraction pattern of cement-emulsified asphalt paste under different proportions for 28 d.

specimens, we found that there was no chemical reaction between asphalt and cement. Moreover, no new mineral phases were formed in the cement hydration products. Thus, only $Ca(OH)_2$ and other characteristic peaks were observed in the patterns of cement-emulsified asphalt; the patterns included all the characteristic peaks of hydration products obtained from cement. Furthermore, characteristic peaks representing new material were not observed in the patterns. When we used different proportions of specimens, the intensity of diffraction peaks representing the specimens was different at different ages; the diffraction peak of X0

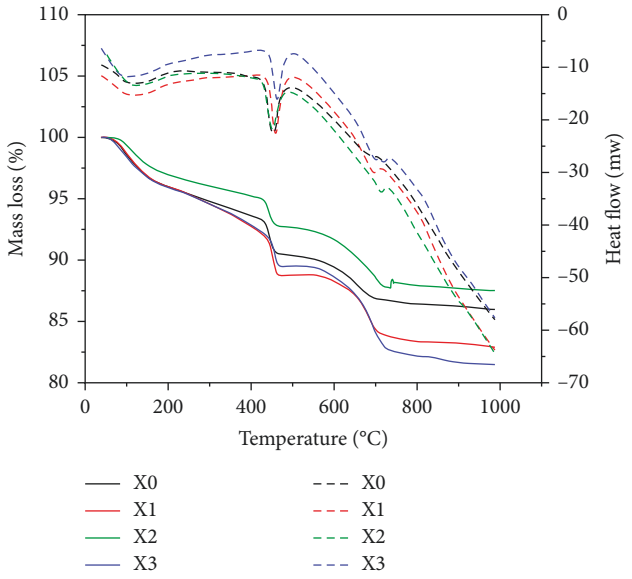

Figure 9: TG-DTA curves of paste specimens with different mix ratios for 7 d.

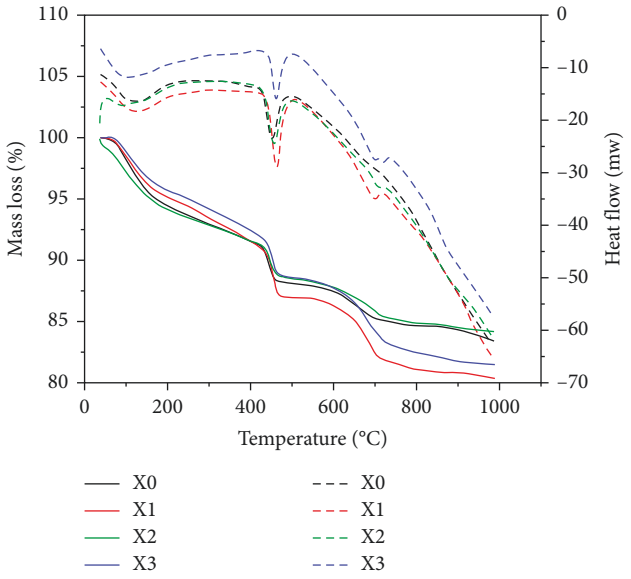

Figure 10: TG-DTA curves of paste specimens with different mix ratios for 28 d.

was higher than that of X1 on the 7th day of ageing; however, the diffraction peak of X0 was slightly lower than that of X1 on the 28th day of ageing. Both these effects were related to the retarding property of the dopant in the emulsified asphalt. Furthermore, there were obvious amorphous peaks of components in the diffraction pattern, and these peaks were observed due to the scattering of asphalt.

3.8. Differential Thermal Analysis (TG-DTA). Table 4 shows the results of differential thermal analysis that was performed on mix proportions of cement-emulsified asphalt concrete. Figures 9–11 illustrate the TG-DTA curves of the cement-emulsified asphalt with different mix ratios on the 7th, 28th, and 90th day of ageing.

The TG curves clearly manifest that the changes in the intensity of peak with respect to the three ages; these changes in peak intensity completely agreed with the changes observed with the variation of temperature. A relatively small loss of mass is observed when the X2 specimen is mixed with single clay. In contrast, a massive loss of mass is observed when the X1 specimen is mixed with single-emulsified asphalt. Moreover, the mass loss gradually increased with the increasing ages, indicating that the hydration reaction of paste samples was becoming more adequate when they were allowed to age for a longer period of time. In the graph, a weak peak appeared from 80°C to 100°C; the peak characterized the dehydration of calcium silicate hydrate and ettringite. A sharp peak was observed between 400°C and 500°C, and this peak represented the endothermic valley of Ca$(OH)_2$ dehydration. Finally, a sharp peak was observed between 650°C and 700°C, and it represented the endothermic valley of $CaCO_3$ decomposition. Despite using different proportions, the hydration products of cement paste were

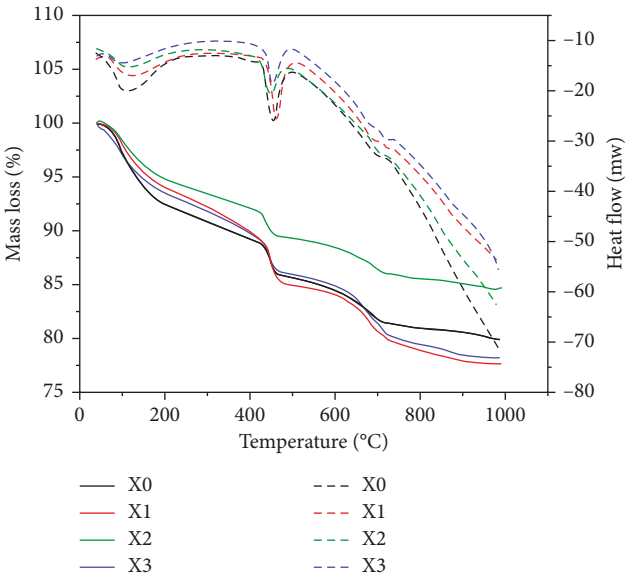

Figure 11: TG-DTA curves of paste specimens with different mix ratios for 90 d.

basically the same as that of X0, but the number of products produced was slightly different.

The DTA curve illustrates that there was a steady decrease in the content of $Ca(OH)_2$ crystals in the X0 specimen at the late stages of analysis. This indicates that $Ca(OH)_2$ is involved in the secondary hydration reaction. In the X1 specimen containing single emulsion asphalt and the X3 composite specimen containing the dopant, the content of $Ca(OH)_2$ increased at the late period. The heat flow of X1 was 23 mw, 30 mw, and 25 mw on the 7th, 28th, and 90th day of ageing, respectively. This indicates that the hydration rate of $Ca(OH)_2$ was relatively slow at the early stage; however, it

increased rapidly at the late stage of analysis. This effect has been attributed to the retarding effect of emulsified asphalt, which is in complete agreement with the above analysis results; the results represent the mechanical properties of concrete.

4. Conclusions

(1) Emulsified asphalt incorporation in concrete delayed the hydration of cement, resulting in relatively slow development of early compressive strength of concrete; the late strength of concrete increased rapidly with the demulsification of emulsified asphalt and hydration of cement. The elastic modulus of plastic concrete is small, and the compressive strength is low. Mixed with emulsified asphalt and clay, the concrete whose compressive strength of 28 d could reach 9 MPa was with lower elastic modulus; the ratio of modulus to strength of the concrete was generally less than 500 and even some below 200, and the deformation capacity was greater than that of the ordinary hydraulic concrete.

(2) The CT mean value analysis of cement-emulsified asphalt concrete specimens showed that the failure process of cement-emulsified asphalt concrete could be divided into 4 stages: compaction, dilatancy, crack propagation, and failure. The volume expansion of each section was not consistent, and the variation of the CT mean value of each section was different; the CT mean value of the place near the lower end face suffered a larger decline but a smaller decline to the upper part of the sample. The evolution of concrete suffering damage to failure is a gradual development process, and no sharp expansion of brittle failure, which further showed that the cement-emulsified asphalt concrete had certain toughness.

(3) There were many pores in the cement-emulsified asphalt paste and a lot of uneven bump on slurry surface. A large number of cement hydration products and some asphalt films which cladded on the surface of the hydration product formed the hardened paste skeleton. The unhydrated cement, asphalt, fibrous C–S–H gel, CH, needle-shaped ettringite, and other hydration products were interwoven to constitute emulsified asphalt-cement paste and to form a spatial structure. There was no chemical reaction between cement and asphalt which produced by demulsification of emulsified asphalt, but there was a retarding effect of emulsified asphalt. The cement-emulsified asphalt concrete has certain plasticity, so we can explore it using in the permanent seepage control engineering under deep overburden.

Conflicts of Interest

The authors confirm that the mentioned funding did not lead to any conflicts of interest regarding the publication of this manuscript. Also there are no other possible conflicts of interest in the manuscript.

Acknowledgments

This work was supported by the National Natural Science Foundation of China (No. 51539002).

References

[1] Y. Li, *Building Materials*, China Water Power Press, Beijing, China, 2001.

[2] Q. Wang, W. Sun, and H. Xiong, *The Plastic Concrete Cut-Off Wall*, China Water Power Press, Beijing, China, 2008.

[3] J. Ouyang, Y. Tan, Y. Li, and J. Zhao, "Demulsification process of asphalt emulsion in fresh cement-asphalt emulsion paste," *Materials and Structures*, vol. 48, no. 12, pp. 3875–3883, 2015.

[4] A. Mahboubi and A. Ajorloo, "Experimental study of the mechanical behavior of plastic concrete in triaxial compression," *Cement and Concrete Research*, vol. 35, no. 2, pp. 412–419, 2005.

[5] C. Zhang, Y. Chen, and Y. Guo, "Clay concrete for cutoff wall in earth dam," *Journal of Hydraulic Engineering*, vol. 36, no. 12, pp. 1464–1469, 2005.

[6] S. Hinchberger, J. Weck, and T. Newson, "Mechanical and hydraulic characterization of plastic concrete for seepage cut-off walls," *Canadian Geotechnical Journal*, vol. 47, no. 4, pp. 461–471, 2010.

[7] A. M. Sha and Z. J. Wang, "Microstructure of mastics-aggregate interface in cement emulsified asphalt concrete," *Journal of Changan University*, vol. 4, p. 28, 2008.

[8] S. F. Brown and D. Needham, "A study of cement modified bitumen emulsion mixtures," in *Association of Asphalt Paving Technologists Proceedings of the Technical Sessions 2000*, White Bear Lake, MN, USA, 2000.

[9] S. Oruc, F. Celik, and M. V. Akpinar, "Effect of cement on emulsified asphalt mixtures," *Journal of Materials Engineering and Performance*, vol. 16, no. 5, pp. 578–583, 2007.

[10] J. Liu, X. Zheng, S. Li et al., "Effect of the stabilizer on bubble stability and homogeneity of cement emulsified asphalt mortar in slab ballastless track," *Construction and Building Materials*, vol. 96, pp. 135–146, 2015.

[11] J. Zhou, F. Dang, H. Chen et al., "Breakage meso mechanism of concrete based on CT test under uniaxial compression," *Journal of Xi'an University of Technology*, vol. 22, no. 4, pp. 335–360, 2006.

[12] Z. X. Wen and F. W. Liu, *Concrete Quality Inspected by Acoustic Nondestructive CT*, Vol. 9, China Three Gorges Construction, Beijing, China, 2002, in Chinese.

[13] W. Tian and F. Dang, "CT image analysis of meso fracture process of concrete," *Engineering Journal of Wuhan University*, vol. 41, no. 2, pp. 69–74, 2008.

[14] Y. Wu, W. Ding, and G. Cao, "Observation and detection of evolution process of rock crack on CT scale under uniaxial and triaxial compression condition," *Journal of Xi'an University of Technology*, vol. 19, no. 2, pp. 115–119, 2003.

[15] J. Ren, X. Ge, Y. Pu, W. Ma, and Y. Zhu, "Primary study of real-time CT testing of unloading damage evolution law of rock," *Chinese Journal of Rock Mechanics and Engineering*, vol. 19, no. 6, pp. 697–701, 2000.

[16] H. Peng and J. Zhang, "The boundary element method for bond—anchorage length," *International Journal Hydroelectric Energy*, vol. 19, no. 2, pp. 85–88, 2001.

[17] A. M. Nevelle, *Properties of Concrete*, Person Education Press, London, UK, 4th edition, 2008.
[18] F. M. Nejad, M. Habibi, P. Hosseini, and H. Jahanbakhsh, "Investigating the mechanical and fatigue properties of sustainable cement emulsified asphalt mortar," *Journal of Cleaner Production*, vol. 156, pp. 717–728, 2017.
[19] T. Rutherford, Z. Wang, X. Shu, B. Huang, and D. Clarke, "Laboratory investigation into mechanical properties of cement emulsified asphalt mortar," *Construction and Building Materials*, vol. 65, no. 13, pp. 76–83, 2014.
[20] Z. Zhao, "Lime active decay law is studied in the lime soil," *Transportation Science and Technology*, vol. 4, pp. 98–100, 2005.
[21] K. J. Mun, W. K. Hyoung, C. W. Lee, S. Y. So, and Y. S. Soh, "Basic properties of non-sintering cement using phosphogypsum and waste lime as activator," *Construction and Building Materials*, vol. 21, no. 6, pp. 1342–1350, 2007.
[22] Z. Wang, *Structure and Performance of the Interface Zone between Mortar and Aggregate in Cement Emulsified Asphalt Concrete*, Chang'an University, Xi'an, China, 2007.
[23] Z. Wang, Q. Wang, and T. Ai, "Comparative study on effects of binders and curing ages on properties of cement emulsified asphalt mixture using gray correlation entropy analysis," *Construction and Building Materials*, vol. 54, pp. 615–622, 2014.